Supporting information

An innovative Z-type Sb$_2$S$_3$/In$_2$S$_3$/TiO$_2$ heterostructure: Superior performance in photocatalytic removal of levofloxacin and mechanistic insight

Jianrou Li, Zhuangzhuang Yin, Jun Guo, Wei Gan, Chen Ruixin, Miao Zhang*, Zhaoqi Sun*

School of Materials Science and Engineering, Anhui University, Hefei 230601, Anhui Province, PR China

* Corresponding author:

Prof. Zhaoqi Sun, E-mail address: szq@ahu.edu.cn

Prof. Miao Zhang, E-mail address: zhmiao@ahu.edu.cn

Text S1. Photocatalytic activity evaluation

High performance liquid chromatography-mass spectrometry (LC-MS, thermofisher, LTQ Orbitrap XL) with an electrospray (ESI) source in positive ionization mode (m/z=50-750) was used to identify the intermediates of LEV photocatalytic degradation. A Waters BEH C18 column (100 mm x 2.1 mm) was used for HPLC separation at 30 °C. The mobile phases A and B utilized were 0.1% formic acid aqueous solution and acetonitrile, and the detergent flow rate was held constant at 0.2 mL/min. The injection volume for the analysis was 20 μL. The linear gradient elution was set as follows: the initial 90% A was reduced to 5% A over 5 min and maintained for 7 min. Then, the mobile phase A was restored to 90% within 1 min and maintained for another 2 min.

Text S2. Free radical capture experiment

Benzoquinone (BQ), isopropyl alcohol (IPA), and disodium ethylenediaminetetraacetate (EDTA-2Na) were selected as the scavengers to trap vacancies (h^+), superoxide radicals ($\cdot O_2^-$), and hydroxyl radicals ($\cdot OH$), respectively. All three trapping agents had a concentration of 1.0 mmol/L. Using the 5,5-dimethyl-1-pyrroline-N-oxide (DMPO) spin trapping reagent for electron paramagnetic resonance (EPR, Bruker EMX Plus), the reactive chemicals $\cdot O_2^-$ and $\cdot OH$ in the photodegradation reaction were examined.

Text S3. Computational details

The LEV removal efficiency is calculated by the Lambert-Beer law in Eq. S1[12,

13]:

$$\eta(\%) = \frac{(C_0/C_t)}{C_0} = \frac{(A_0/A_0)}{A_0} \times 100 \tag{S1}$$

where η denotes the removal efficiency; C_0 and C_t denote the initial and instantaneous concentrations of LEV (mg/L), respectively; A_0 and A_t are the absorbance at 0 and t min, respectively.

The photodegradation curve of LEV was fitted by the quasi primary reaction kinetic Eq. S2[12-14]:

$$-ln\left(\frac{C_t}{C_0}\right) = kt \tag{S2}$$

Here, C_0 and C_t denote the initial and instantaneous concentrations of LEV (mg/L), respectively; k is the kinetic constant; and t is the degradation time (min).

The optical band gap of a photocatalyst can be calculated from its optical absorption spectrum according to the following Eq. S3 [2, 12, 13, 15, 16]:

$$ahv = A(hv - E_g)^{n/2} \tag{S3}$$

Where, a is the absorption coefficient, h is Planck's constant, v is the incident light frequency (Hz), A is the proportionality constant, E_g is the optical band gap energy (eV), and the value of n depends on the semiconductor transition type decision, with n values of 1 and 4 representing direct and indirect absorption, respectively.

The work function of the catalysts can be obtained by the calculation method below Eq. S4 [15, 16]:

$$\emptyset = hv - |E_{cutoff} - E_F| \tag{S4}$$

Where the hv represents the photon energy of the excitation light used for

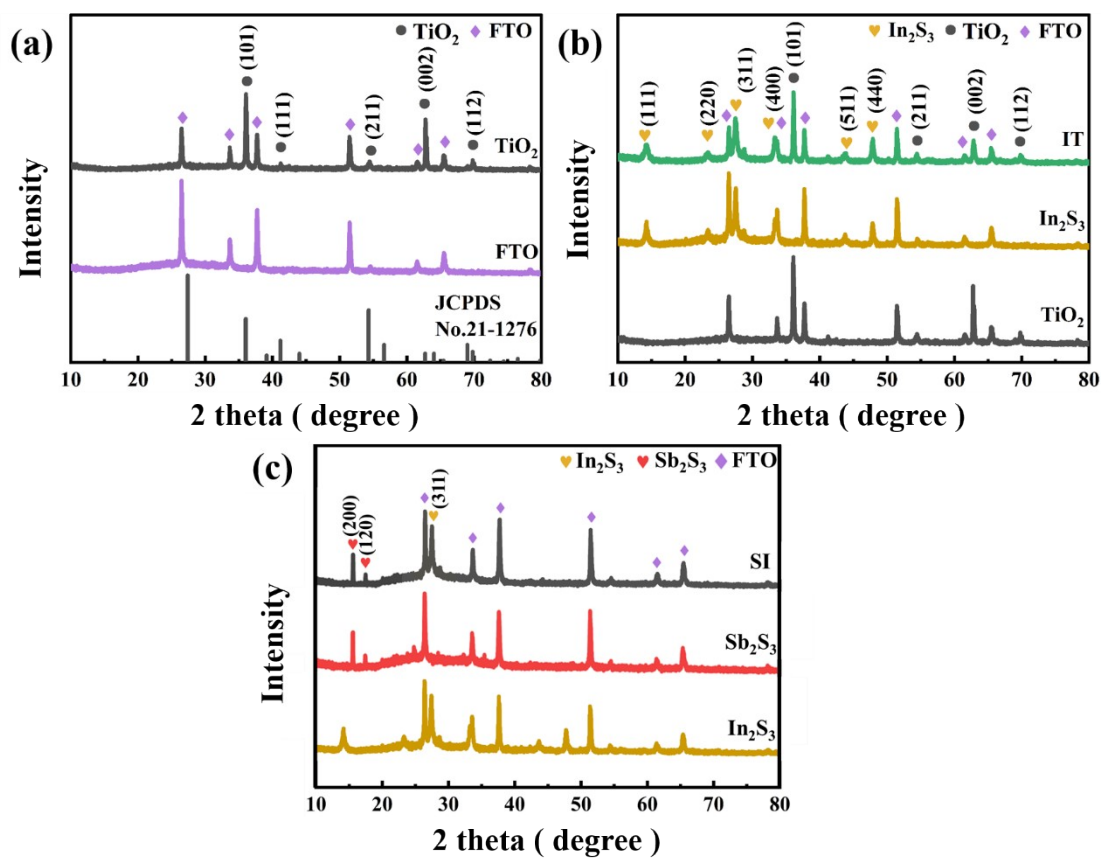detection (21.21 eV), the E_{cutoff} represents the cutoff energy.

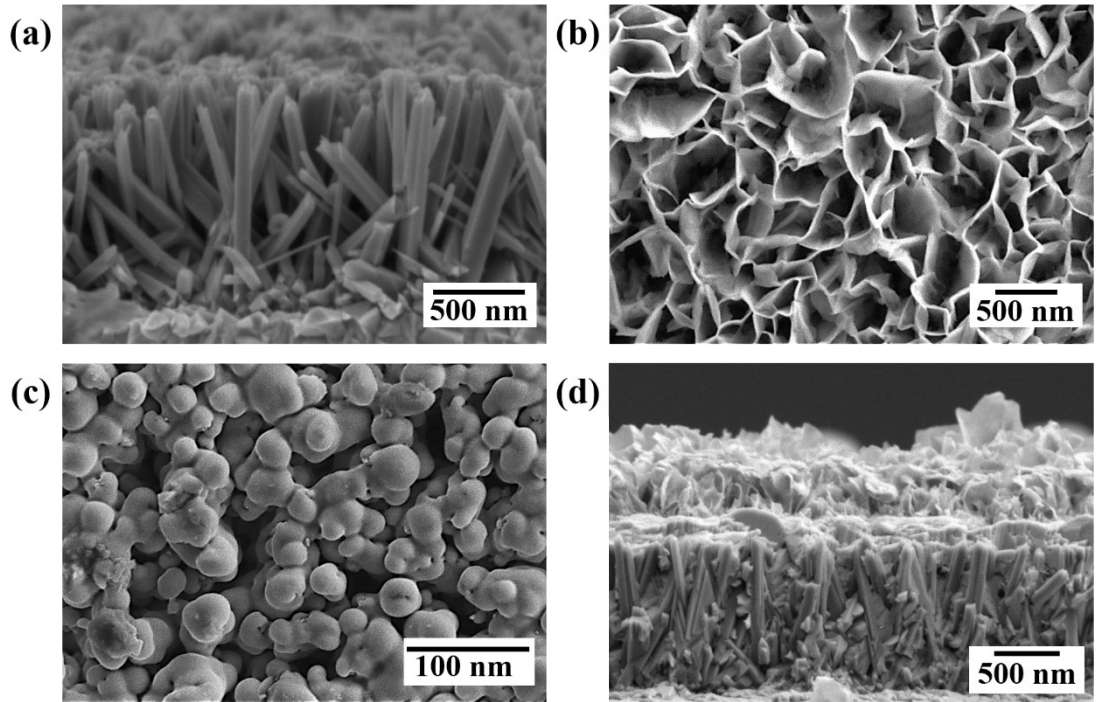**Fig. S1** XRD patterns of pure TiO$_2$ (a), IT (b) and SI (c).

Fig. S2 SEM images of TiO_2 (a) cross section, In_2S_3 (b), Sb_2S_3 (c) and SIT cross sections.
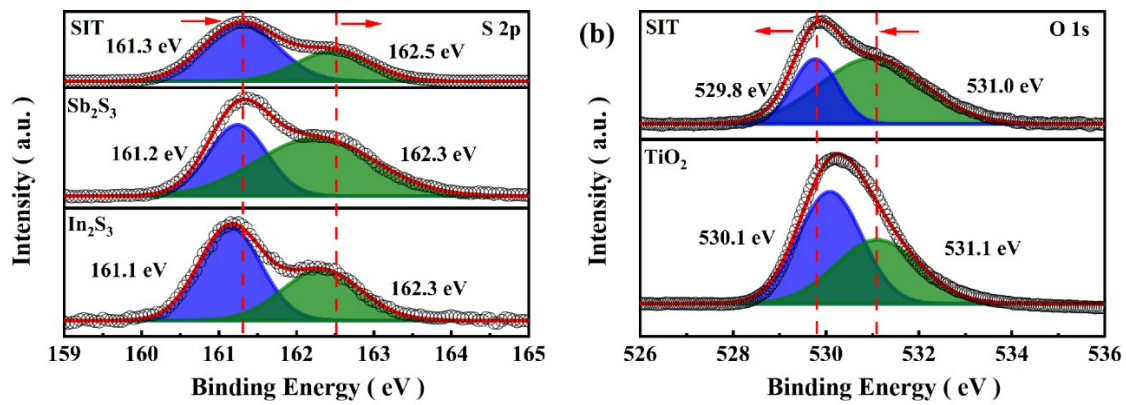
Fig. S3 XPS spectra of the high-resolution spectra of S 2p(a) and O 1s.
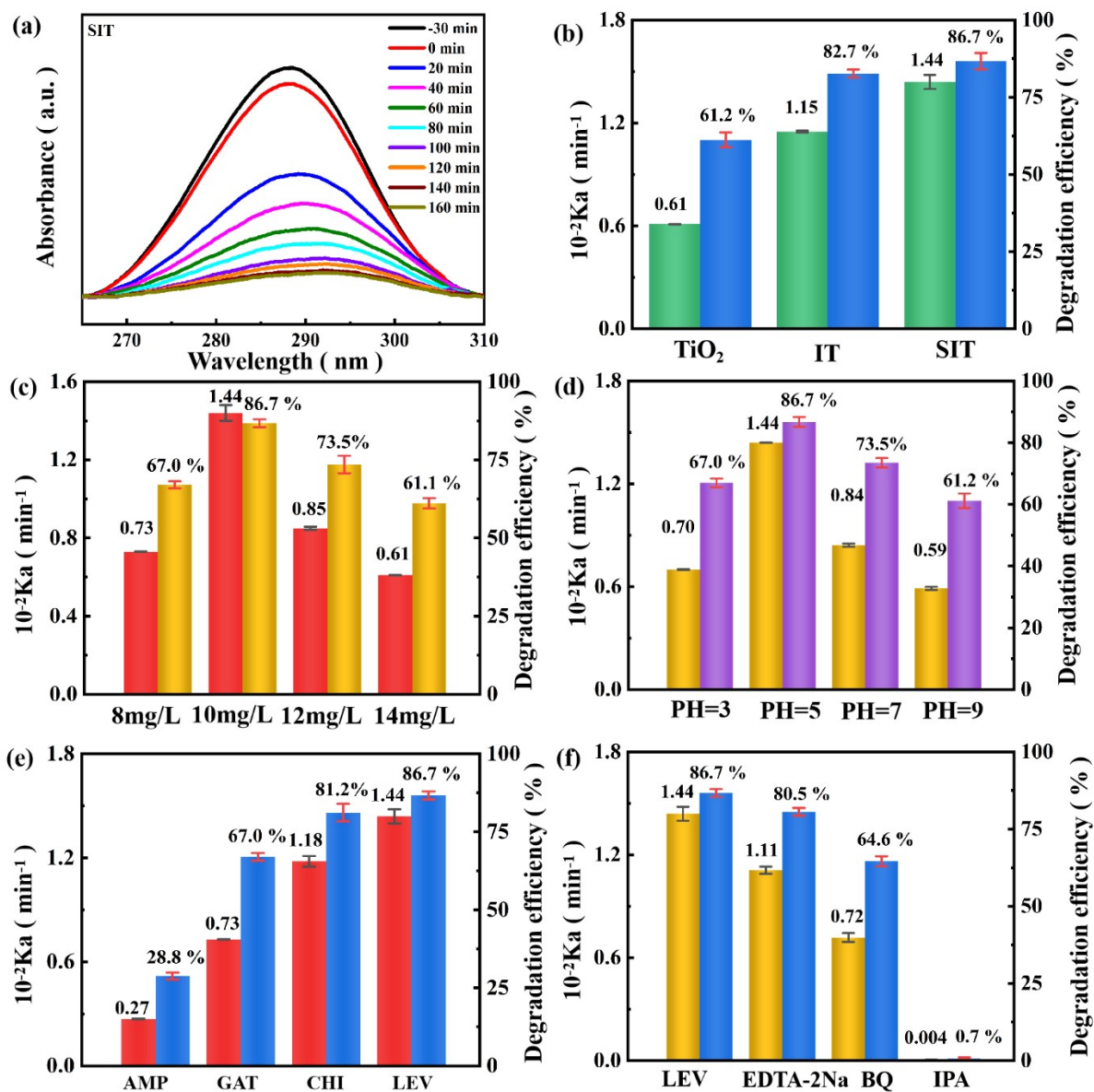
Fig. S4 The UV–vis spectra of LEV degradation by SIT at different reaction time(a);

the apparent constant and degradation efficiency of different catalysts(b), different

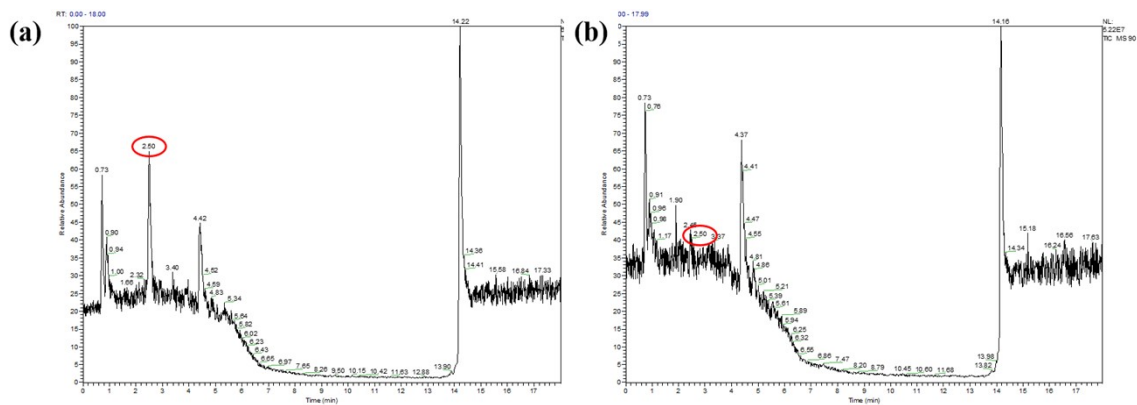LEV concentration(c), different initial pH(d), different antibiotics(e) and different free

radical trapping(f).

Fig. S5 MS spectra of LEV (Reaction conditions: [LEV] = 10 mg/L; [photocatalyst size] = 1 cm × 1 cm; pH = 7; T = 25∘C).
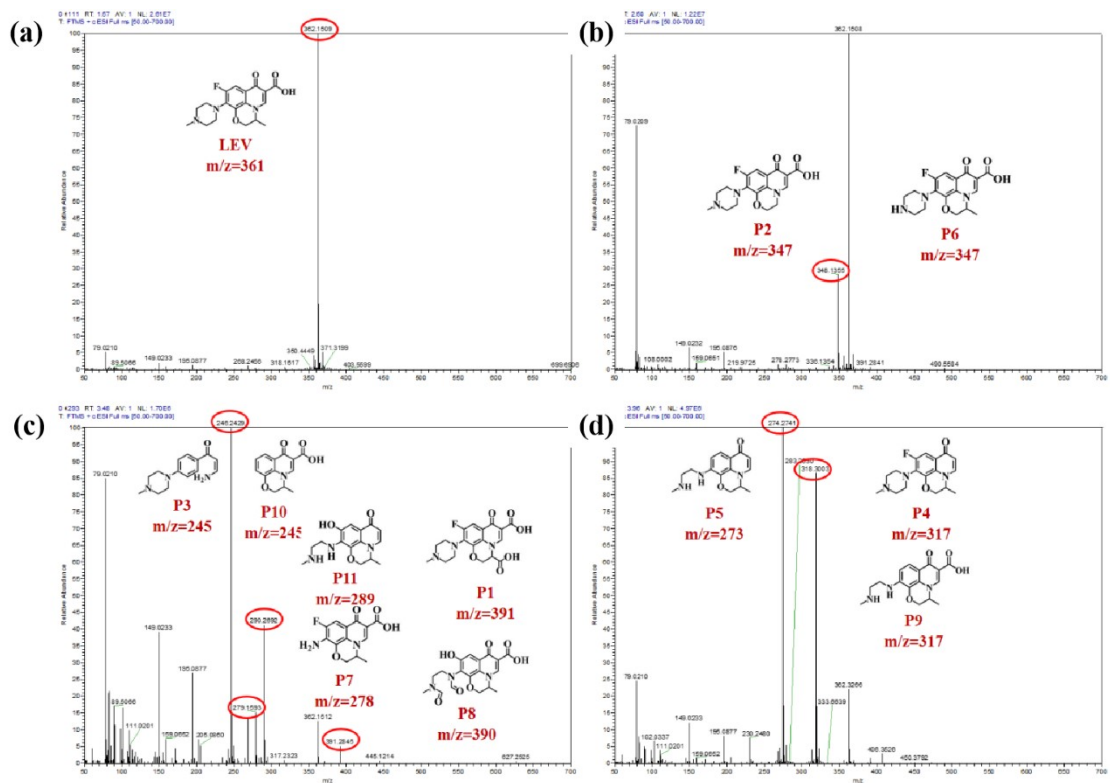
Fig. S6 LC-MS spectra of LEV degradation with different retention time (a) 0 min, (b) 40 min, (c) 80min, (d) 120min.
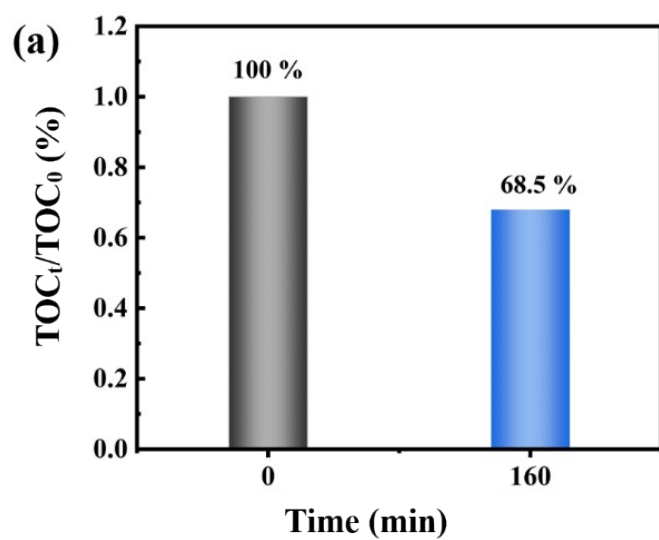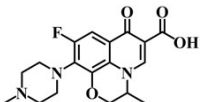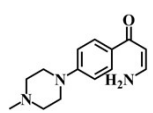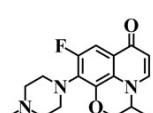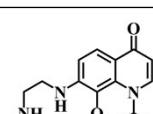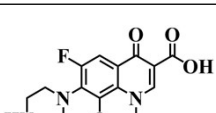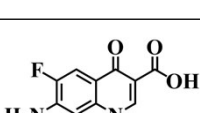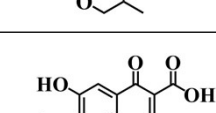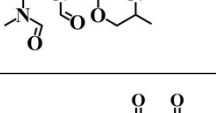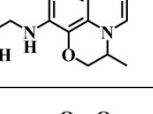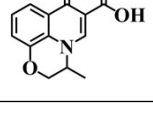
Fig. S7 Mineralization of LEV by SIT.
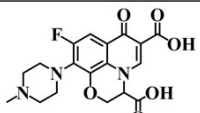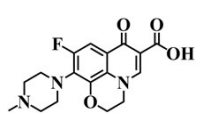
Table. S1 Detailed information of LEV degradation intermediates.

Compounds	m/z	Formula	Proposed structure	References
LEV	361	$C_{18}H_{20}FN_3O_4$		[1-3]
P1	391	$C_{18}H_{18}FN_3O_6$		[2, 4, 5]
P2	347	$C_{17}H_{18}FN_3O_4$		[1, 5]
P3	245	$C_{14}H_{19}N_3O$		[6]
P4	317	$C_{17}H_{20}FN_3O_2$		[5, 7]
P5	273	$C_5H_6O_5$		[5]
P6	347	$C_{17}H_{18}FN_3O_4$		[8, 9]
P7	278	$C_{13}H_{11}FN_2O_4$		[1, 3, 10]
P8	390	$C_{18}H_{19}N_3O_7$		[11]
P9	317	$C_{15}H_{19}N_3O_2$		[5]
P10	245	$C_{13}H_{11}NO_4$		[6]
P11	289	$C_{15}H_{19}N_3O_3$		[11]

References

[1] J. Shen, L. Qian, J. Huang, Y. Guo, Z. Zhang, Enhanced degradation toward Levofloxacin under visible light with S-scheme heterojunction In_2O_3/Ag_2CO_3: Internal electric field, DFT calculation and degradation mechanism, Sep. Purif. Technol., 275 (2021) 119239. http://doi.org/10.1016/j.seppur.2021.119239

[2] C. Ding, Y. Lu, J. Guo, W. Gan, S. Qi, Z. Yin, M. Zhang, Z. Sun, Internal electric field-mediated sulfur vacancies-modified-In_2S_3/TiO_2 thinfilm heterojunctions as a photocatalyst for peroxymonosulfate activation: Density functional theory calculations, levofloxacin hydrochloride degradation pathways and toxicity of intermediates, Chem. Eng. J., 450 (2022) 138271. http://doi.org/10.1016/j.cej.2022.138271

[3] J. Nie, X. Yu, Z. Liu, Y. Wei, J. Zhang, N. Zhao, Z. Yu, B. Yao, Boosting principles for the photocatalytic performance of Cr-doped Cu_2O crystallites and mechanisms of photocatalytic oxi-dation for levofloxacin, Appl. Surf. Sci., 576 (2022) 151842. http://doi.org/10.1016/j.apsusc.2021.151842

[4] Z.-T. Dong, C.-G. Niu, H. Guo, H.-Y. Niu, S. Liang, C. Liang, H.-Y. Liu, Y.-Y. Yang, Anchoring $CuFe_2O_4$ nanoparticles into N-doped carbon nanosheets for peroxymonosulfate activation: Built-in electric field dominated radical and non-radical process, Chem. Eng. J., 426 (2021) 130850. http://doi.org/10.1016/j.cej.2021.130850

[5] Q. Deng, X. Zhang, L. Chang, H. Chai, Y. Huang, The MOF/LDH derived

heterostructured $Co_3O_4/MnCo_2O_4$ composite for enhan-ced degradation of levofloxacin by peroxymonosulfate activatio-n, Sep. Purif. Technol., 294 (2022) 121182. http://doi.org/10.1016/j.seppur.2022.121182

[6] J. Jiang, X. Wang, C. Yue, S. Liu, Y. Lin, T. Xie, S. Dong, Efficie-nt photoactivation of peroxymonosulfate by Z-type nitrogen-defect-rich $NiCo_2O_4$/g-C_3N_4 for rapid emerging pollutants degra-dation, J. Hazard. Mater., 414 (2021) 125528. http://doi.org/10.1016/j.jhazmat.2021.125528

[7] X. Zhang, Y. Zhang, X. Jia, N. Zhang, R. Xia, X. Zhang, Z. Wang, M. Yu, In situ fabrication of a novel S-scheme heterojunction photocatalyts Bi_2O_3/P-C_3N_4 to enhance levofloxacin removal fro-m water, Sep. Purif. Technol., 268 (2021) 118691. http://doi.org/10.1016/j.seppur.2021.118691

[8] J. Cai, Y. Zhang, T. Qian, X. Li, Z. Chen, L. Zhang, Bismuth oxybromide/bismuth oxyiodide nanojunctions decorated on flexible carbon fiber cloth as easily recyclable photocatalyst for removing various pollutants from wastewater, J. Colloid Interface Sci., 608 (2022) 2660-2671. http://doi.org/10.1016/j.jcis.2021.10.188

[9] C.K. Tsai, Y.C. Lee, T.T. Nguyen, J.J. Horng, Levofloxacin degradation under visible-LED photo-catalyzing by a novel ternary Fe-ZnO/WO_3 nanocomposite, Chemosphere, 298 (2022) 134285. http://doi.org/10.1016/j.chemosphere.2022.134285

[10] Q. Jin, D. Ji, Y. Chen, Z. Tang, Y. Fu, Kinetics and pathway of levofloxacin

degradation by ferrate(VI) and reaction mechanism of catalytic degradation by copper sulfide, Sep. Purif. Technol., 282 (2022) 120104. http://doi.org/10.1016/j.seppur.2021.120104

[11] L. He, S. Yang, S. Shen, Y. Ma, Y. Chen, J. Xue, J. Wang, L. Zheng, L. Wu, Z. Zhang, L. Yang, Novel insights into the mechanism of periodate activation by heterogeneous ultrasonic-enhanced sludge biochar: Relevance for efficient degradation of levofloxacin, J. Hazard. Mater., 434 (2022) 128860. http://doi.org/10.1016/j.jhazmat.2022.128860

[12] J. Guo, W. Gan, C. Ding, Y. Lu, J. Li, S. Qi, M. Zhang, Z. Sun, Black phosphorus quantum dots and Ag nanoparticles co-modified TiO_2 nanorod arrays as powerful photocatalyst for tetracycline hydrochloride degradation: Pathways, toxicity assessment, and mechanism insight, Sep. Purif. Technol., 297 (2022) 121454. http://doi.org/10.1016/j.seppur.2022.121454

[13] C. Ayappan, V. Jayaraman, B. Palanivel, A. Pandikumar, A. Mani, Facile preparation of novel Sb_2S_3 nanoparticles/rod-like α-Ag_2WO_4 heterojunction photocatalysts: Continuous modulation of band structure towards the efficient removal of organic contaminants, Sep. Purif. Technol., 236 (2020) 116302. http://doi.org/10.1016/j.seppur.2019.116302

[14] S. Sharma, S. Basu, Fabrication of centimeter-sized Sb_2S_3/SiO_2 monolithic mimosa pudica nanoflowers for remediation of hazardous pollutants from industrial wastewater, Journal of Cleaner Production, 280 (2021) 124525.

http://doi.org/10.1016/j.jclepro.2020.124525

[15] Y. Chen, Y. Cheng, J. Zhao, W. Zhang, J. Gao, H. Miao, X. Hu, Construction of $Sb_2S_3/CdS/CdIn_2S_4$ cascaded S-scheme heteroju-nction for improving photoelectrochemical performance, J. Coll-oid Interface Sci., 627 (2022) 1047-1060. http://doi.org/10.1016/j.jcis.2022.07.117

[16] J. Zhao, Y. Cheng, Y. Chen, W. Zhang, E. Liu, J. Fan, H. Miao, X. Hu, Defects regulation of Sb_2S_3 by construction of Sb_2S_3/In_2S_3 direct Z-type heterojunction with enhanced photoelectro-chemical performance, Appl. Surf. Sci., 568 (2021) 150917. http://doi.org/10.1016/j.apsusc.2021.150917